International Journal of Mechanical Sciences 144 (2018) 887–896

Contents lists available at ScienceDirect

International Journal of Mechanical Sciences

journal homepage: www.elsevier.com/locate/ijmecsci

A confinement-dependent load-induced thermal strain constitutive model for concrete subjected to temperatures up to 500 °C

Giacomo Torelli[a,*], Parthasarathi Mandal[b], Martin Gillie[c], Van-Xuan Tran[d]

[a] Department of Engineering, University of Cambridge, Cambridge CB2 1PZ, UK
[b] School of Mechanical, Aerospace and Civil Engineering, The University of Manchester, Manchester M13 9PL, UK
[c] School of Engineering, University of Warwick, Coventry CV4 7AL, UK
[d] EDF Energy, R&D UK Centre, 40 Grosvenor Place, SW1×7EN, London UK

ARTICLE INFO

Keywords:
Concrete
Temperature
Fire
Load-induced thermal strain
LITS
Transient thermal creep
Stress confinement

ABSTRACT

This paper proves that, given a Load-Induced Thermal Strain (LITS) curve able to accurately describe the uniaxial LITS development for a specific type of concrete and temperatures up to 500 °C, a more accurate prediction of the 3D LITS state is obtained through a confinement-dependent 3D implementation than through the classic confinement-independent approach. In particular, a new model is presented, obtained by extending to 3D a fourth order polynomial LITS derivative function in a way that allows the effects of the stress confinement to be taken into account. For comparison purposes, the same fourth order polynomial LITS derivative function is also implemented in 3D through the classic confinement-independent modelling approach. These constitutive relationships are adopted to model transient experiments performed on concrete subjected to constant uniaxial and biaxial compressive loads. The results show that the confinement-dependent modelling approach gives a better prediction of the LITS state developing in the case of biaxial compression than the classic confinement-independent approach. Finally, the validated confinement-dependent model is applied to evaluate the LITS-related stress redistribution taking place in a typical Prestressed Concrete Pressure Vessel (PCPV) subjected to heating to 500 °C and cooling back to the normal operating temperature of 50 °C. It is found that including the effects of three dimensional LITS behaviour has significant effects on the predicted stress states.

1. Introduction

When heated in the absence of mechanical load, concrete exhibits an isotropic expansion usually referred to as Free Thermal Strain (FTS). However, experimental evidence shows that if concrete is subjected to a compressive load while heated, a different thermal strain is measured. The difference between the thermal strain measured in the case of mechanically loaded concrete and the FTS is commonly termed Load Induced Thermal Strain (LITS). Many authors have demonstrated that LITS develops in the direction of the compressive load and is mainly irrecoverable on cooling or unloading [1–8].

Since the magnitude of LITS is of the same order as FTS, developing and implementing robust numerical concrete constitutive laws that include LITS is crucial for reliable modelling of the behaviour of concrete subjected to heating-cooling cycles. In this regard, it has been demonstrated that LITS plays a key role, particularly in the case of structural elements whose thermal deformation is partially or totally constrained, where significant tensile stresses and associated cracking effects may result from LITS during cooling [9].

Over the last four decades, many authors experimentally studied LITS developing in uniaxially loaded concrete. Such loading conditions are relevant for one-dimensional members, as are common in concrete frame structures. Based on uniaxial transient tests, many models have been proposed where LITS is considered as a quasi-instantaneous strain component and is expressed as a nonlinear function of stress and temperature history.

Commonly, 3D LITS models are based on the assumption of the superimposition principle [10–15]; in other words it is assumed that the LITS state that develops in the case of multiaxial confinement equals the sum of the LITS states corresponding to each compressive stress component applied individually. However, the few multiaxial tests that are available in the literature show that the situation is more complex and LITS depends on the confinement of the stress state [8,16]. For this reason, a novel approach for modelling LITS as a stress-confinement strain component has been presented by the authors in [17]. The model was

* Corresponding author.
E-mail address: gt384@cam.ac.uk (G. Torelli).

https://doi.org/10.1016/j.ijmecsci.2017.12.054
Received 30 November 2016; Received in revised form 30 November 2017; Accepted 31 December 2017
Available online 4 January 2018
0020-7403/

validated for temperatures up to 250 °C, temperatures representative of nuclear Prestressed Concrete Pressure Vessels (PCPVs) subjected to partial fault of their water cooling system. The validation studies were performed using experimental data from Petkovski and Crouch [8]. This work showed that accounting for the effects of stress confinement was important for accurately calculating stress-states in bulk concrete structures such as PCPVs used in nuclear power stations. In the present paper, the 3D extension method proposed by the authors in [17] is adopted for formulating a LITS model able to capture the behaviour of multiaxially confined concrete subjected to transient temperatures up to 500 °C, temperatures representative of nuclear PCPVs subjected to complete fault of their water cooling system. The approach is validated and discussed in the light of the experimental studies by Kordina et al. [16].

2. Confinement-dependent LITS model for temperatures up to 500 °C

2.1. Confinement-dependent 3D implementation method

A number of 3D LITS models have been formulated by assuming that LITS develops isotopically. Accordingly, such models are based on a formal analogy with the 3D Hooke's law [10–15]:

$$\dot{\varepsilon}_{ij}^{\text{lits}} = \frac{\beta(T)}{\sigma_{u0}}(-\upsilon_{\text{lits}}\sigma_{kk}^{-}\delta_{ij} + (1+\upsilon_{\text{lits}})\sigma_{ij}^{-})\dot{T} \tag{2.1}$$

Where a $\beta(T)$ is the LITS function, i.e. a generic function of temperature aimed at fitting the uniaxial temperature-LITS curve, σ_{u0} the compressive strength of the material, $\sigma_{ij}{}^{-}$ is the (i,j)th component of the negative projection of the stress tensor and υ_{lits} a material parameter analogous to the elastic Poisson's ratio ν. It is worth noting that the approach reported in Eq. (2.1) is based on the superposition principle and treats LITS as a confinement-independent phenomenon. In other words, according to this formulation the LITS in a multiaxially loaded specimen is obtained as the sum of the LITS states produced by each mechanical load component independently.

This assumption is in contrast with the results of the only two sets of experiments involving transient thermal conditions applied under multiaxial compression known by the authors [8,16]. An analysis of these results shows that the experimentally measured LITS state under multiaxial conditions exceeds that predicted by merely superimposing uniaxial LITS states [19]. This has been explained by postulating the confinement-dependency of the two main driving mechanism of LITS, namely micro cracking and micro diffusion [17].

For this reason, the approach of taking the stress confinement into account presented by the authors in [17] has been adopted in this work. The method consists of including the dependency of LITS on the confinement of stress state in (2-1) by introducing a confinement coefficient η:

$$\dot{\varepsilon}_{ij}^{\text{lits}} = \eta\frac{\beta(T)}{\sigma_{u0}}(-\upsilon_{\text{lits}}\sigma_{kk}^{-}\delta_{ij} + (1+\upsilon_{\text{lits}})\sigma_{ij}^{-})\dot{T} \tag{2.2}$$

Where σ_{ij}^{-} is the ith jth component of the negative projection $\overline{\overline{\sigma}}^{-}$ of the stress tensor $\overline{\overline{\sigma}}$. The confinement coefficient η is automatically evaluated at each time step as a function of the negative projections of principal stresses σ_1^{-}, σ_2^{-} and $\sigma_3^{-}$and of a user-defined triaxiality scaling factor γ:

$$\eta = 1 + (C_m - 1)\gamma \tag{2.3}$$

$$C_m = \frac{\left|\sigma_1^{-} + \sigma_2^{-} + \sigma_3^{-}\right|}{\sqrt{(\sigma_1^{-})^2 + (\sigma_2^{-})^2 + (\sigma_3^{-})^2}} \tag{2.4}$$

Where C_m is referred to as triaxiality index.

2.2. Uniaxial LITS function for temperatures up to 500 °C

The confinement-dependent method presented in Eq. (2.2), (2.3) and (2.4) was previously employed by the authors to implement a 3D LITS function that varied bi-linearly with temperature aimed at capturing the development of LITS for temperatures up to 250 °C [17]. The bilinear LITS curve was obtained by defining a constant LITS derivative function $\beta(T) = B$ and by ensuring that LITS did not develop for temperatures lower than a user-defined critical temperature, T_{CRIT}. In this model, the critical temperature T_{CRIT} represents the experimentally observed temperature threshold of 100 °C above which LITS starts developing significantly [8]. Such a bilinear curve was conceived as a simple and effective alternative to the more complex LITS functions available in the literature, valid for applications involving temperatures up to 250 °C [20–22]. One notable application case is the assessment of nuclear power plants in the case of a partial fault of the cooling system [17]. However, this bilinear LITS model fails to capture the markedly nonlinear development of LITS for higher temperatures. As a consequence, for applications involving temperatures higher than 250 °C, more complex uniaxial LITS curves need to be adopted.

Many uniaxial models have been proposed in the past, where LITS is formulated as a polynomial function of temperature by curve-fitting the uniaxial tests for temperatures up to 600 °C [20,22]. In this work, the uniaxial LITS curve has been defined as a fifth-order polynomial of the temperature. The order of the polynomial was chosen by gradually increasing the degree of the polynomial adopted to curve fit the experimental LITS data reported in Fig. 1 until a good fit was obtained. This approach has previously been adopted by Terro, who demonstrated the suitability of fifth-order polinomials to match experimental LITS curves obtained for various concrete mixes [22]. Accordingly, the confinement-dependent 3D extension method described in the Section 2.1 has been applied to a fourth-order LITS derivative function $\beta(T)$:

$$\beta(T) = b_0 + b_1 T + b_2 T^2 + b_3 T^3 + b_4 T^4 \tag{2.5}$$

Where the polynomial coefficients b_0, b_1, b_2, b_3 and b_4 have to be chosen so that $\beta(T)$ fits the uniaxial LITS curve in the loaded direction. Table 1 presents different sets of coefficients for various types of concrete, which were obtained by fitting data, presented by a range of authors via polynomial regression. The corresponding LITS curves were plotted in Fig. 1. These curves can be adopted in the case of a predictive calculation, where it is not possible to test the considered concrete mix. For concrete mixes whose properties are unknown, a range of calculations, based on the different curves presented in Fig. 1 or their envelopes could be performed, in order to analyse a potential range of material behaviours. It should be noted that the sets of coefficients reported in Table 1 for various concrete mixes can be reasonably considered independent of the stress level. This is because experimental evidence shows that LITS can be modelled as directly proportional to stress for moderate load levels [18,23].

3. Constitutive relationship including LITS

A thermoelastic constitutive relationship including LITS has been implemented in the finite element solver *Code_Aster* [24], through the code generator *MFront* [25].

3.1. Implementation of the LITS model

The LITS model has been obtained by combining the confinement-dependent 3D implementation approach described by Eq. (2.2), (2.3) and (2.4) with the polynomial LITS function $\beta(T)$ defined in Eq. (2.5). This model has been developed so that LITS results only on first heating under compressive load, in accordance to experimental evidence [1–8]. This has been achieved by storing the maximum temperature ever reached by the material in an internal variable T_{MAX} and imposing the

Table 1
Different sets of polynomial coefficients to be adopted for various types of concrete. Coefficients calibrated by curve fitting the experimental data obtained by a range of authors: (a) Kordina et al. [16], (b) Mindeguia et al. [7], (c) Khoury et al. [18], (d) Brite Euram III [11], (e) Anderberg et al. [23].

Polynomial coefficients	(a) Kordina et al. [16]	(b) Mindeguia et al. [7]	(c) Khoury et al. [18]	(d) Brite Euram III [11]	(e) Anderberg et al. [23]
b_0 [°C^{-1}]	2.70E−05	5.42E−05	5.19E−06	−2.14E−05	−7.30E−06
b_1 [°C^{-1}]	−1.02E−06	−1.51E−06	−8.26E−07	−7.79E−08	−8.14E−07
b_2 [°C^{-1}]	6.12E−09	8.73E−09	5.45E−09	−1.15E−10	6.40E−09
b_3 [°C^{-1}]	−1.26E−11	−1.85E−11	−1.31E−11	4.69E−12	−1.57E−11
b_4 [°C^{-1}]	6.92E−15	1.09E−14	9.11E−15	−1.08E−14	1.06E−14

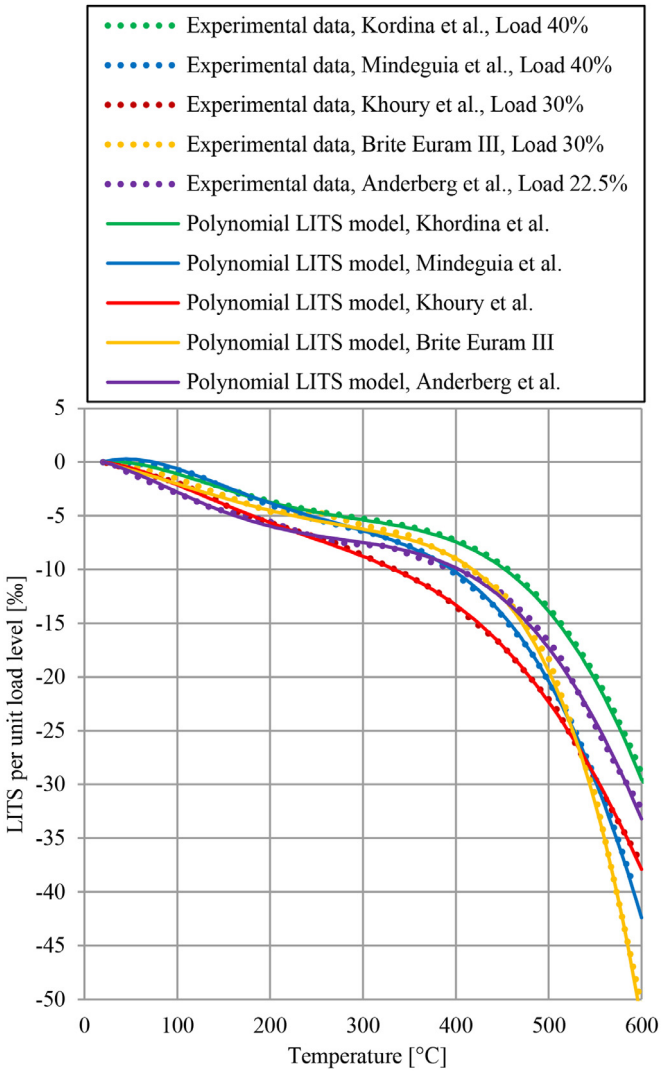

Fig. 1. Experimental LITS data, per unit load level, presented by various authors (Kordina et al. [16], Mindeguia et al. [7], Khoury et al. [18], Brite Euram III [11], Anderberg et al. [23]) and LITS curves obtained by means of 4th order polynomial functions of the temperature $\boldsymbol{\beta(T)}$ calibrated via polynomial regression.

increment in LITS tensor $\Delta\bar{\bar{\varepsilon}}_{\text{lits}}$ over a generic time step to be null for temperatures lower than T_{MAX}:

$$\begin{cases} \Delta\bar{\bar{\varepsilon}}_{\text{lits}} = 0 & \text{for } T \le T_{\text{MAX}} \\ \Delta\bar{\bar{\varepsilon}}_{\text{lits}} = \eta\left[\frac{\beta(T)}{\sigma_{u0}}\right]\left(\left(1+\upsilon_{\text{lits}}\right)\bar{\bar{\sigma}}_{\overline{m}} - \upsilon_{\text{lits}} tr\left(\bar{\bar{\sigma}}_{\overline{m}}\right)\bar{\bar{I}}\right)\Delta T & \text{for } T = T_{\text{MAX}} \end{cases} \tag{3.1}$$

Where $\bar{\bar{\sigma}}^{-}_{m}$ is the mean value of the negative projection of the stress tensor over the considered time step. Such value is obtained as the mean of the negative projection of the stress tensor at the beginning of the time step $\bar{\bar{\sigma}}^{-}_{ini}$ and at the end of the time step $\bar{\bar{\sigma}}^{-}_{\text{fin}}$.

Similarly, the triaxiality index C_m defined in Eq. (2.4) was implemented as a function of the mean values $\sigma^{-}_{1,\text{m}}$, $\sigma^{-}_{2,\text{m}}$ and $\sigma^{-}_{3,\text{m}}$ of the principal stresses over the time step:

$$C_m = \frac{\left|\sigma^{-}_{1,\text{m}} + \sigma^{-}_{2,\text{m}} + \sigma^{-}_{3,\text{m}}\right|}{\sqrt{\left(\sigma^{-}_{1,\text{m}}\right)^2 + \left(\sigma^{-}_{2,\text{m}}\right)^2 + \left(\sigma^{-}_{3,\text{m}}\right)^2}} \tag{3.2}$$

3.2. General strain decomposition

The implemented 3D LITS model has been included in a thermo-elastic constitutive relationship. This resulted in the following general strain decomposition:

$$\Delta\bar{\bar{\varepsilon}}_{\text{tot}} = \Delta\bar{\bar{\varepsilon}}_{\text{ela}} + \Delta\bar{\bar{\varepsilon}}_{\text{fts}} + \Delta\bar{\bar{\varepsilon}}_{\text{lits}} \tag{3.3}$$

Where $\Delta\bar{\bar{\varepsilon}}_{\text{tot}}$, $\Delta\bar{\bar{\varepsilon}}_{\text{ela}}$, $\Delta\bar{\bar{\varepsilon}}_{\text{fts}}$ and $\Delta\bar{\bar{\varepsilon}}_{\text{lits}}$ are the increment in total strain, elastic strain, FTS and LITS, respectively:

$$\Delta\bar{\bar{\varepsilon}}_{\text{ela}} = \frac{1+\upsilon}{E}\Delta\bar{\bar{\sigma}} - \frac{\upsilon}{E} tr(\Delta\bar{\bar{\sigma}})\bar{\bar{I}} \tag{3.4}$$

$$\Delta\bar{\bar{\varepsilon}}_{\text{fts}} = \alpha\Delta T\bar{\bar{I}} \tag{3.5}$$

Where $\bar{\bar{I}}$ is the identity matrix, $\Delta\bar{\bar{\sigma}}$ is the stress tensor increment, E is the Young's modulus, υ the Poisson's ratio and α is the coefficient of thermal expansion.

3.3. Numerical methods

The mechanical material model defined in Sections 3.1 and 3.2 has been adopted for static nonlinear mechanical analyses via the finite element software *Code_Aster* [24] through a *Newton–Raphson* iterative method with tangent matrix prediction [26,27]. The material behaviour law has been implemented by the code generator *MFront* [25]. Locally, the constitutive law is integrated by means of an implicit procedure based on a *Newton–Raphson* method and a jacobian matrix obtained through a second order finite difference [25]. The model implemented here could be easily included in more comprehensive concrete material models that include damage, plasticity and creep as required. This is because the implicit scheme used for the local integration of the material behaviour law allows additional strain components to be directly added to the general strain decomposition described in Eq. (3.3).

4. Verification studies

The LITS model described in Sections 2 and 3 has been calibrated and verified by modelling transient tests performed by Kordina et al. [16] on concrete specimens subjected to uniaxial and biaxial stress states. The objective of these studies was to compare the strain predictions obtained by the traditional method of calculating LITS based on superposition, and the herein implemented confinement-dependent method for temperatures up to 500 °C.

4.1. Reference experiments

The reference tests consisted of rectangular parallelepiped-shaped concrete specimens subjected to thermal transients under constant uniaxial or biaxial loading conditions [16]. The mechanical loads were applied through four hydraulic cylinders, each with a maximum force of

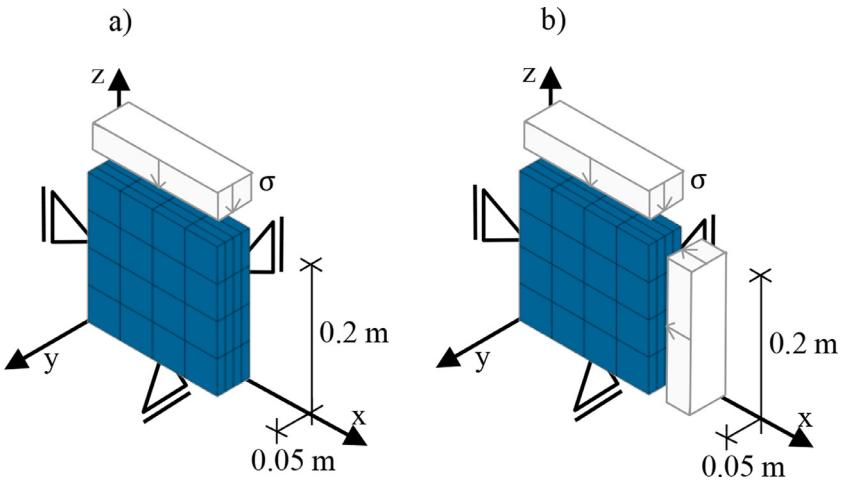

Fig. 2. Mesh, boundary and loading conditions defined for modelling the transient tests reported in [16]: (a) Uniaxial compression (b) Equal biaxial compression.

1000 kN, placed at the inner surface of a high stiffness loading frame. The thermal load was applied by an electrical furnace, while keeping the mechanical load constant.

The sizes of the specimens and loading platens were chosen so as to obtain stress states as close to an ideal biaxial condition as possible. In particular, concrete specimens having a thickness of 50 mm were sawn out of concrete cubes having an edge length of 200 mm. This resulted in $200 \times 200 \times 50$ mm parallelepiped-shaped concrete specimens that were loaded "in-plane", that is, in the directions of their long edges. Moreover, the restraining friction between loading platens and specimen surfaces was minimized by applying the compressive forces by means of loading-brushes constructed as proposed in [28]. A relatively slow heating rate of 2 °C/min was chosen to guarantee a reasonably homogeneous temperature field throughout the specimen during the thermal transient. This choice was made to prevent the appearance of substantial thermal gradients through the specimens, owing to structural effects [29]. In this regard, other authors have found that, provided that the heating rate is lower than 5 °C/min, it has little or no influence on the development of LITS [18,23,29,30]. On the other hand, heating rates higher than 5 °C/min have been found to cause premature collapses and explosions [29].

Temperatures, forces and strains were recorded continuously during the tests. The temperatures were measured by thermocouples applied to the surfaces of the specimen. The forces in the specimens were measured through four load cells located between the cylinders and the specimens, while the deformations occurring on heating were monitored directly by a high-temperature measuring device composed of inductive displacement transducers and deformation transmitters arranged along the three axes. The LITS curve corresponding to a specific load level was obtained indirectly as the difference between the total thermal strain curve measured for a loaded specimen and the free thermal strain measured for an identical unloaded control specimen subjected to the same thermal load. According to this definition, LITS implicitly includes the increment in elastic strain undergone by loaded concrete subjected to transient thermals.

4.2. Finite element models

The specimens were meshed using 64 hexahedral finite elements with 8 nodes, with 4 elements along the three directions (Fig. 2). This resulted in a relatively refined mesh along the thickness of the specimens, allowing the thermal gradients developing in this direction during the thermal transient to be accurately captured. Kinematic boundary conditions were applied so that the specimens were able to deform along the three axis without rigid body motions. The three faces lying on the planes $x = 0$ mm, $y = 0$ mm and $z = 0$ mm were prevented from translation in their normal directions, while all the other nodes of the models were not constrained. A uniformly distributed pressure σ was applied to the faces lying on the planes $x = 200$ mm and $z = 200$ mm for modelling equal biaxial compressive stress states, while only the face at $z = 200$ mm was mechanically loaded for modelling uniaxial compressive conditions.

Prior to performing mechanical analyses, a nonlinear thermal analysis was conducted to evaluate the evolution of the temperature field throughout the specimen during the thermal transient. The thermal conductivity λ and volumetric specific heat c_v were defined as temperature-dependent parameters, according to the recommendations provided by the Eurocode 2 [31]. The thermal conductivity curve $\lambda(T)$ was defined as the average of the upper and lower limit functions provided by the recommendation. The water evaporation process was implicitly taken into account by taking the specific heat capacity as a function of temperature $c_p(T)$, as proposed by Eurocode 2 for an initial moisture content of 3% by weight. The thermal load was modelled by imposing a constant rise in temperature to all the nodes lying on the external surfaces of the specimen under constant mechanical loads. A heating rate of 2 °C/min was adopted, equal to the experimental one [16].

The thermal expansion coefficient $\alpha(T)$ was defined as the derivative of a 6-th order polynomial interpolation of the experimental FTS curve with respect of the temperature. The polynomial coefficients of the LITS derivative function $\beta(T)$ and the LITS Poisson's ratio were calibrated only on the basis of uniaxial LITS curves. Specifically the coefficients of $\beta(T)$ were calibrated so as to match the uniaxial LITS curve, in the direction of the load, for a load level σ/σ_{u0} of 40%. It should be noted that, since the experimental LITS curves obtained for different load levels present small differences in shape, a slightly different calibration would have been obtained if $\beta(T)$ had been defined to exactly match the LITS curve shape corresponding to a load level σ/σ_{u0} of 20%. A LITS Poisson's ratio of 0.48 was chosen based on the experimentally observed ratio between transversal and axial deformation for uniaxial compressive stresses. In this study, a constant Young's modulus of 47,000 MPa was adopted. The heating-induced increment in elastic strain component, usually modelled by defining a temperature-dependent Young's modulus, is here implicitly included in the LITS model. This is because the LITS model is calibrated against LITS curves including such a temperature-driven increment in elastic strain, as discussed in Section 4.1. Accordingly, if a temperature-dependent Young's modulus was defined, the variation of elastic properties with temperature would be taken into account twice.

A traditional and a confinement-dependent version of the LITS model were adopted here. In practice, the results corresponding to the traditional method were obtained by employing the implemented

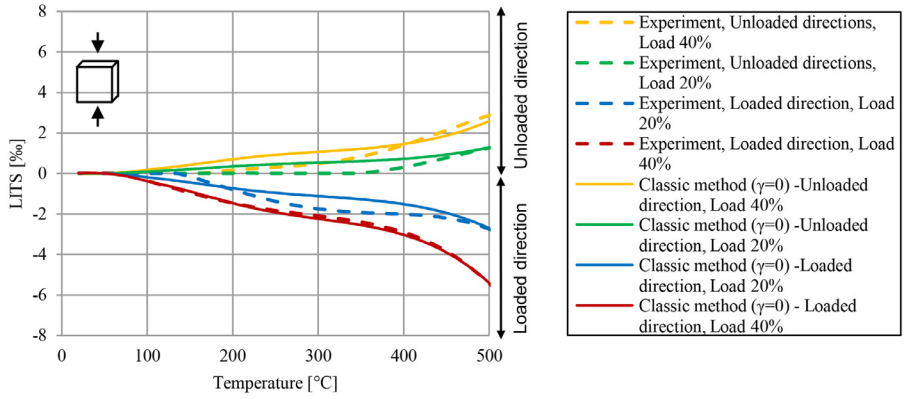

Fig. 3. Comparison between experimental uniaxial LITS curves [16] and numerical results obtained with the traditional 3D implementation method. Curves obtained in the loaded and unloaded directions, for uniaxial compression and load levels σ/σ_{u0} of 20% and 40%.

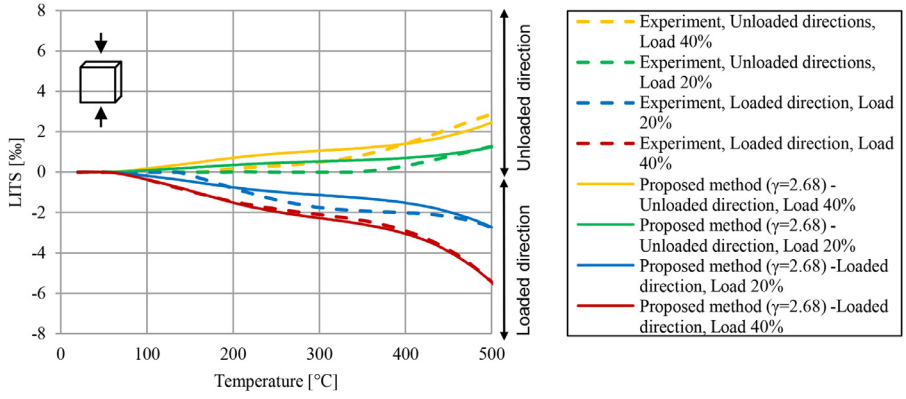

Fig. 4. Comparison between experimental uniaxial LITS curves [16] and numerical results obtained with the proposed confinement-dependent 3D implementation method. Curves obtained in the loaded and unloaded directions, for uniaxial compression and load levels σ/σ_{u0} of 20% and 40%.

Table 2
Material parameters adopted in the simulations with LITS implemented in 3D via (a) Traditional and (b) Confinement-dependent methods.

Material parameter	(a) Traditional method	(b) Confinement-dependent method
E	47,000 MPa	47,000 MPa
ν	0.25	0.25
b_0	2.93×10^{-5} °C^{-1}	2.93×10^{-5} °C^{-1}
b_1	-1.10×10^{-6} °C^{-1}	-1.10×10^{-6} °C^{-1}
b_2	6.65×10^{-9} °C^{-1}	6.65×10^{-9} °C^{-1}
b_3	-1.37×10^{-11} °C^{-1}	-1.37×10^{-11} °C^{-1}
b_4	7.51×10^{-15} °C^{-1}	7.51×10^{-15} °C^{-1}
σ_{u0}	57 MPa	57 MPa
ν_{lits}	0.48	0.48
γ	0	2.68

confinement-dependent formulation described in the previous sections and setting a triaxiality scaling factor $\gamma = 0$. This is because for $\gamma = 0$ the confinement coefficient η defined in (2-3) equals 1, for any loading condition, therefore reducing the confinement-dependent implementation method described by Eq. (2.2) to the traditional method described by Eq. (2.1). By contrast, the confinement-dependent version of the LITS model was obtained by setting a triaxiality scaling factor γ of 2.8, identified as the value matching the experimentally obtained LITS loaded direction for biaxial compression and a load level σ/σ_{u0} of 40%. The employed material parameters are summarized in Table 2.

4.3. Results and discussion

Figs. 3 and 4 show a comparison between experimental uniaxial LITS curves, and numerical results obtained via traditional method and confinement-dependent method, respectively. As expected, the same predictions were obtained in the case of traditional and confinement-dependent method, for uniaxial stress states. This is because, for this particular loading condition ($\sigma_1 \neq 0$, $\sigma_2 = \sigma_3 = 0$), the triaxiality index C_m defined in Eq. (2.4) equals 1, and the confinement coefficient η defined in (2-3) equals 1 for any value of the triaxiality scaling factor γ.

By contrast, significantly different LITS were predicted by the two implementation methods when modelling tests performed under biaxial compressive condition (Figs. 5 and 6). Fig. 5 shows that, if the traditional 3D implementation method is employed, the absolute value of the LITS curves is significantly underestimated for all the analysed cases. This tendency was observed both in the loaded and unloaded directions, for the considered load levels σ/σ_{u0} of 20% and 40%.

The general trend of the experimental LITS curves was better captured when the confinement-dependent model was adopted, as shown by Fig. 6. In this case, a particularly accurate assessment of the LITS developing in the loaded direction was obtained for both the considered load levels of 20% and 40%. A significant improvement in the LITS prediction with respect to the traditional method was also obtained in the unloaded direction, for a load level of 20%. For a load level of 40%, the LITS development obtained in the unloaded direction was more accurate the than the one obtained with the traditional method for temperatures up to 400 °C. However, an overestimation of the experimental results in the unloaded direction was obtained above this temperature. This is mainly due to differences in shape of the experimental LITS curves in the loaded and unloaded direction, which is not captured by either the traditional or the confinement-dependent model. Specifically, the LITS in the unloaded direction increases less markedly than the one measured in the loaded direction for temperatures above 400–450 °C. A possible explanation for this is that due to the simultaneous presence of two

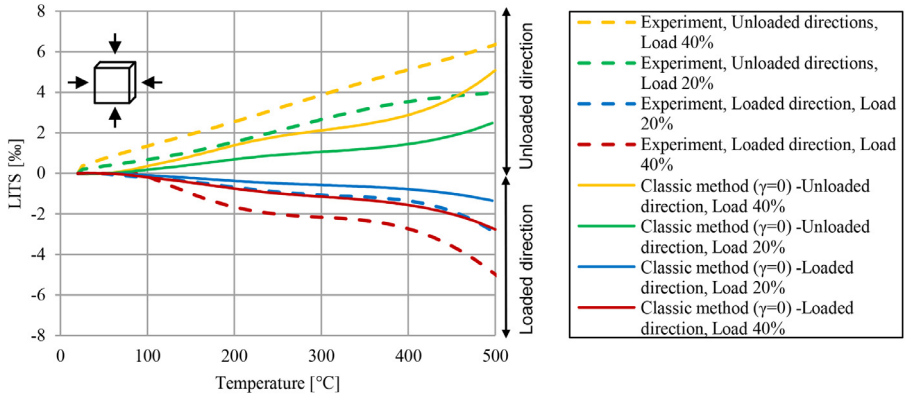

Fig. 5. Comparison between experimental biaxial LITS curves [16] and numerical results obtained with the traditional 3D implementation method. Curves obtained in the loaded and unloaded directions, for biaxial compression and load levels σ/σ_{u0} of 20% and 40%.

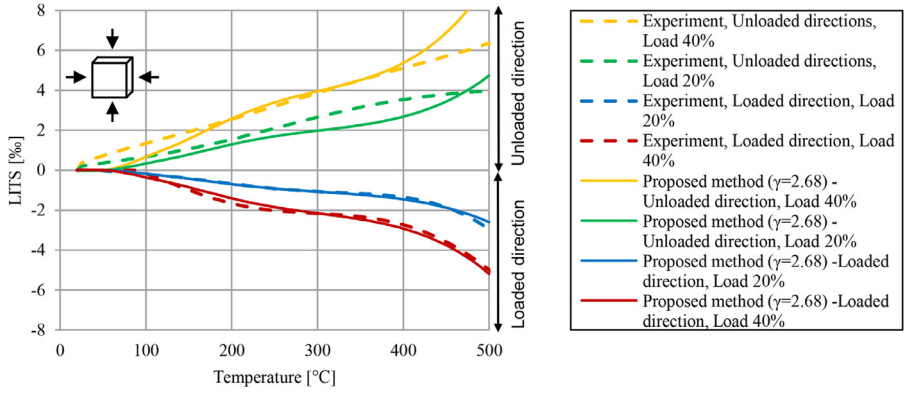

Fig. 6. Comparison between experimental biaxial LITS curves [16] and numerical results obtained with the proposed confinement-dependent 3D implementation method. Curves obtained in the loaded and unloaded directions, for biaxial compression and load levels σ/σ_{u0} of 20% and 40%.

compressive principal stresses, the micro cracking mechanism driving the development of LITS in the unloaded direction starts taking place for lower temperatures than in the case of uniaxial compression. This might result in a relatively early development of LITS in the unloaded direction and, consequently, in a more steady increase of transversal LITS with temperature in the case of biaxial compression. Nevertheless, due to the scarcity of data, caution must be applied in the interpretation of these results and more experimental work is needed to fully understand these mechanisms. Overall, the LITS prediction obtained by the confinement-dependent 3D implementation method was significantly more accurate than the one obtained by the traditional method.

The results of biaxial tests simulations have been also plotted in terms of total thermal strain, i.e. FTS plus LITS, as a function of temperatures (Figs. 7 and 8). For all of the reported load levels and strain directions, LITS can be seen as the difference between the considered thermal strain curve and the FTS curve, corresponding to the total thermal strain curve in absence of load. Fig. 7 shows that, if the traditional method is implemented, the total thermal stain in the two loaded directions is overestimated, while it is underestimated in the unloaded direction. The comparison between Figs 6 and 7 demonstrates that the proposed method generally gives better results in terms of total thermal strain.

5. Study of a PCPV subjected to heating-cooling cycle to 500 °C

The 3D constitutive model presented in the previous sections has been applied to assess the behaviour of a typical PCPV of a nuclear Advanced Gas-cooled Reactor (AGR) under severe accidental conditions. AGRs are a type of nuclear reactors where graphite is used as the neutron moderator and carbon dioxide as gas coolant. In these reactors, the gas coolant circulates through the core and is contained by a PCPV. Under normal operating conditions, the temperature of the gas coolant reaches 500–600 °C, while the temperature of concrete is kept constant at about 50 °C by a cooling pipes system located into the PCPV, close to its internal surface. In the case of a complete fault in the cooling system, the temperature of concrete next to the internal surface of the vessel could rise to the temperature of the gas coolant. In this study, a temporary complete fault of the cooling pipes system was considered. The effect of the fault duration on the structural behaviour of a typical PCPV is investigated by considering two reference fault durations of 2 and 14 days, referred to as *short term* and *long term* fault, respectively. During the faults, the temperature of the internal surface of the PCPV was assumed to be 500 °C.

5.1. FE model

A typical nuclear PCPV was considered, having 5-meters-thick walls and a pre-tensioning system composed of vertical and hoop tendons – see Fig. 9. The prestressing system was modelled as composed of 8 layers of tendons uniformly distributed through the thickness of the wall. As shown from Fig. 9, the structural behaviour of the lateral wall was studied by considering a representative portion located at mid height of the wall itself. A similar approach was adopted in [17].

The representative portion was modelled as a parallelepiped having dimensions 0.5 m × 0.5 mm × 4.5 m, therefore neglecting the effects of radius of the relatively small curvature of the wall itself – see Fig. 9. The concrete matrix was modelled by hexahedral elements, while the tendons were explicitly modelled by bar elements whose nodes were defined as perfectly bonded to the concrete matrix. An initial prestress level of 920 kN was applied to the tendons. The constraining effect of

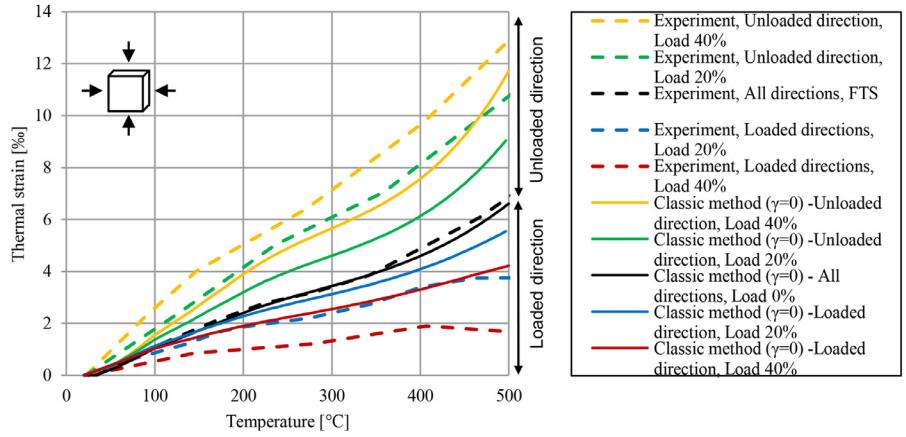

Fig. 7. Comparison between experimental biaxial FTS curves [16] and numerical results obtained with the traditional 3D implementation method. Curves obtained in the loaded and unloaded directions, for load levels σ/σ_{u0} of 20% and 40%.

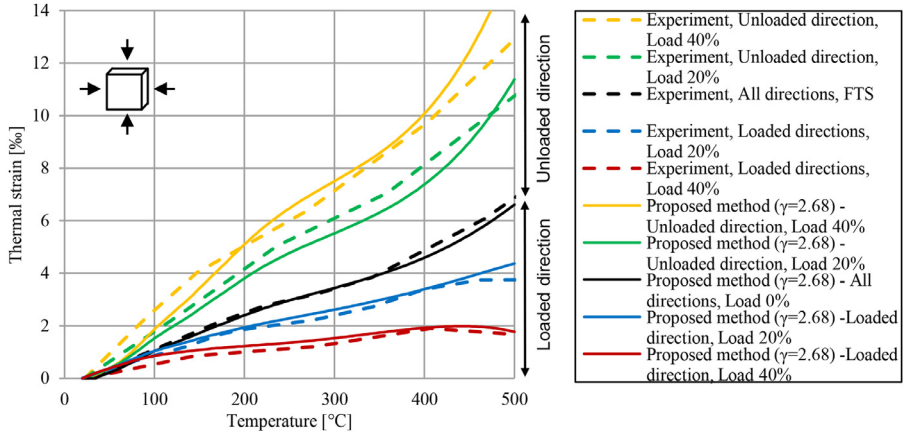

Fig. 8. Comparison between experimental biaxial FTS curves [16] and numerical results obtained with the proposed confinement-dependent 3D implementation method. Curves obtained in the loaded and unloaded directions, for load levels σ/σ_{u0} of 20% and 40%.

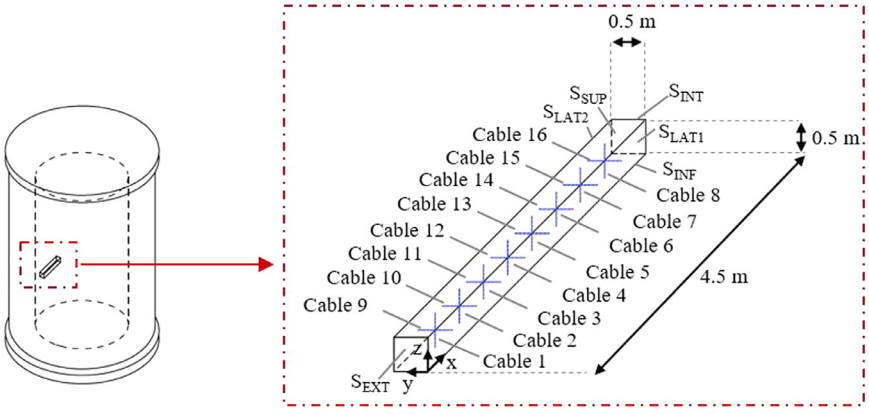

Fig. 9. Typical PCPV geometry and studied representative portion. Adapted from [17].

top cap and foundation were assumed to be negligible at mid-height of the lateral wall [32]. Therefore, kinematic boundary conditions were defined so as to allow the representative elements to expands along the three directions *x, y, z*. With reference to Fig. 9, the faces S_{INT}, S_{LAT1} and S_{INF} were prevented from translating along their normal directions, while all the other nodes were allowed to rotate and translate along any direction. The temporary complete fault of the cooling pipes system was modelled by applying a heating-cooling cycle to the inner surface of the vessel. The temperature histories applied to the internal surface in the cases of *short* and *long* term fault conditions are shown in Fig. 11 and Fig. 13, respectively.

First, two nonlinear thermal analysis were performed to assess the evolution of the temperature field through the wall thickness, for the *short* and *long* term fault conditions. For the thermal analyses, the presence of steel tendons was disregarded. Thermal conductivity and volumetric specific heat were defined according to the Eurocode 2 [31], using the same approach described in Section 4.2 for the validation studies.

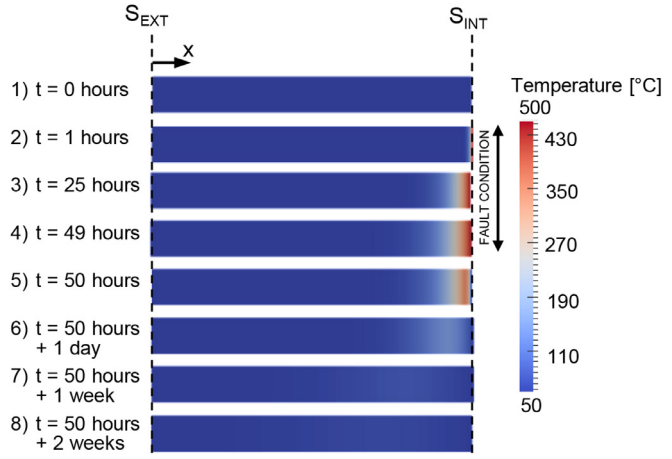

Fig. 10. Evolution of the temperature field though the thickness of the PCPV lateral wall. *Short term* fault condition (2 days). $x(S_{EXT})$=0m, $x(S_{INT})$=5 m.

Then, mechanical analyses were performed to assess the loss in prestress due to the applied heating-cooling cycles. The steel of the tendons was modelled as an elastic material, having Young's modulus $E = 200{,}000$ MPa, Poisson's ratio $\nu = 0.3$ and coefficient of thermal expansion $\alpha = 8 \times 10^{-6}\,°C^{-1}$. In order to investigate the effects of LITS and its confinement dependency on the behaviour of the PCPV under fault conditions, three different material models were considered for the concrete:

- A thermoelastic constitutive law including the confinement-dependent LITS model presented in Sections 2 and 3. In this case the LITS triaxiality scaling factor $\gamma = 2.68$ calibrated against experiments was adopted - see the adopted material parameters in Table 2.
- A thermoelastic constitutive law including a traditional confinement-independent LITS model. As for the validation studies, this material model was obtained by employing the confinement-dependent implementation proposed here and setting a LITS triaxiality scaling factor $\gamma = 0$ - see the adopted material parameters in Table 2.
- A thermoelastic constitutive law without LITS model. This material model was obtained by totally deactivating the LITS component in the material law presented in Sections 2 and 3.

5.2. Results and discussion

Due to their massive structure, PCPVs are capable of absorbing heat efficiently in the case of a fault of the cooling pipes system. Therefore, if the fault is temporary, only a first layer of the wall is significantly affected by the temperature rise at the internal surface of the vessel. Figs. 10 and 12 show the evolution of the temperature field though the thickness of the wall for *short* and *long* term fault conditions, respectively. As expected, the temperature fields obtained demonstrate the duration of the fault significantly influences the extent of heated portion of the PCPV lateral wall, which ranges from about *1* m in the case of a *short* term fault to about *2* m in the case of a *long* term fault.

The results of the mechanical analyses are reported Figs. 11 and 13 in terms of evolution of the tension in *Cable 8,* the closest cable to the inner surface of the vessel (Fig. 9). As a reference, the evolution of the temperature at the inner surface and at *Cable 8* are also reported in these two charts.

Fig. 11 shows the results of *short* term fault analyses. It can be observed that, if the no LITS model is used, an increase in tension in cable number 8 is predicted during the heating phase, due to the difference in FTS of the two materials. On cooling, the increase in tension is completely recovered, due to the perfect-recoverability of the thermal expansions. If LITS is included, a significant stress relaxation is obtained

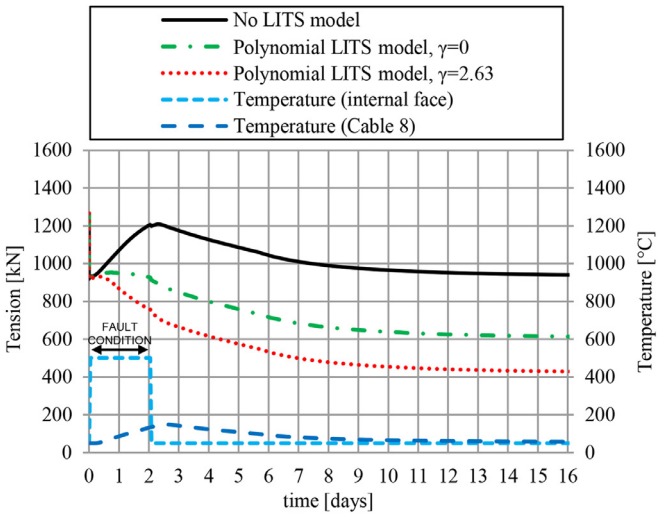

Fig. 11. Loss in tension in Cable 8 obtained without LITS in the constitutive model, with LITS implemented by traditional method (γ=0) and confinement-dependent method (γ=2.68); evolution of the temperature at the inner surface of the vessel and at Cable 8. *Short term* fault condition (2 days).

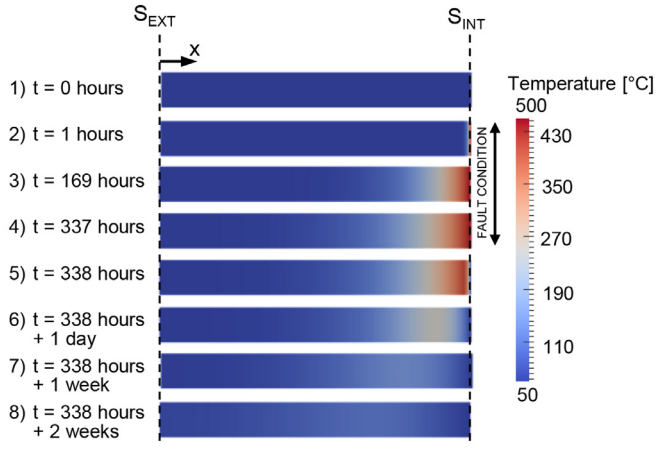

Fig. 12. Evolution of the temperature field though the thickness of the PCPV lateral wall. *Long term* fault condition (14 days). $x(S_{EXT})$=0m, $x(S_{INT})$=5 m.

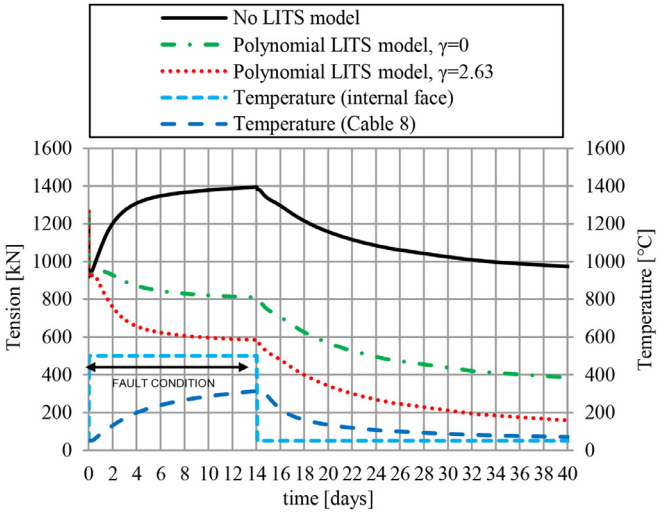

Fig. 13. Loss in tension in Cable 8 obtained without LITS in the constitutive model, with LITS implemented by traditional method (γ=0) and confinement-dependent method (γ= 2.68); evolution of the temperature at the inner surface of the vessel and at Cable 8. *Long term* fault condition (2 days).

on heating, which is not recovered on cooling. This phenomenon is determined by the development of an irrecoverable LITS contraction in the concrete, which leads to a contraction of the tendons and, consequently, to a loss in pretension. Fig. 11 also shows that a substantially bigger drop in tension is predicted by the confinement-dependent method ($\gamma = 2.68$) than the traditional method ($\gamma = 0$). This is because the presence of radial and hoop prestressing tendons causes a biaxial compressive stress state, therefore making the stress confinement effect play a key role in the mechanical behaviour of the material. The loss in pretension at the end of the heating-cooling cycle is 56% and 36% of the initial tension, for the confinement-dependent ($\gamma = 2.68$) and traditional ($\gamma = 0$) methods, respectively. In other words, about 36% of the loss in prestress predicted by considering the confinement dependency of LITS is missed if the traditional method is adopted.

The results of *long* term fault analyses are reported in a similar form in Fig. 13. As expected, bigger drops in tension are obtained than in the case of a *short* term fault, if LITS is taken into account. This is mainly because higher temperatures are reached in the proximities of *Cable 8* and a bigger portion of the wall is affected by the thermal transient, therefore making the constraining effect of the unheated portion of the wall less effective.

The development of LITS during the heating phase leads to a contraction of concrete, which in turn produces a loss of tension in *Cable 8*. A further drop in tension is obtained during the heating phase due to the recovery of the thermal strains of both concrete and steel. The sharp drop in tension observed for all the considered constitutive laws at the beginning of the cooling phase is driven by the relatively quick cooling of the material at *Cable 8*. In this case, the overall losses in tension obtained with confinement-dependent and traditional methods are 89% and 65% of the initial tensions respectively. Therefore, for long term fault conditions, about 28% of the tension loss assessed by considering the confinement effect is missed when the traditional method is employed.

It is worth noting that, in the case of a *long* term fault, the adoption of the traditional method leads to a slightly smaller underestimation of the tension loss than in the case *short* term fault. This is because, for this particular type of application, LITS development and the compressive stress level are coupled. At a material level, at the beginning of the heating phase, the ratio between the LITS developments per unit increase in temperature obtained by the confinement-dependent method and by traditional method correspond to the confinement coefficient η. However, as the temperature increases, this ratio decreases, since in the confinement-dependent LITS model, the material is subjected to lower stress than in the case of the confinement-independent one. Therefore, the LITS development with temperature obtained by these two different models cannot be considered proportional. Since higher temperatures are reached in the case of long term fault conditions, a slightly smaller underestimation of LITS is obtained if the traditional method is used.

The results of these studies show that the development of LITS in the concrete of a PCPV subjected to an accidental heating-cooling cycle leads to a significant stress redistribution along the thickness of the vessel wall. It is also shown that if LITS is not modelled as confinement-dependent, non-conservative estimates of the stress and strain states are obtained. Specifically, it was found that in the case of *long* term fault conditions, the development of LITS could lead to losses in pretension of 80–90% in the closest cables to the inner surface of the vessel. However, these findings must be interpreted with caution for two main reasons. First, the predicted loss in pretension of 80–90% is a local phenomenon, which affects only a relatively thin layer of wall. This might significantly affect the behaviour of the liner-concrete interface at the inner surface of the wall but not jeopardize the global structural performances of the reactor. Second, these results have been obtained by implementing the presented LITS model in a basic thermoelastic material behaviour law. This means that damage, plasticity and creep effects are not taken into account here. Even though the initial stress state of the vessel justifies the adoption of an elastic material behaviour law, a more precise prediction of the stress redistribution taking place on heating would be predicted by implementing the presented LITS model in a more comprehensive material behaviour law. This is because the thermal gradients through the thickness of the wall that develop on heating determine the appearance of significant compressive and tensile stresses. In particular, the first layer of material is heated first and tends to expand, causing significant tensile stresses in the colder inner material, which tends to expand less. Such tensile stresses could lead to local cracking effects which are not accounted for here, therefore affecting the predicted loss in prestress in the tendons.

6. Conclusions

This paper presents a confinement-dependent 3D LITS model for concrete, to be used for temperatures up to 500 °C. The LITS model is obtained by combining a fourth order polynomial LITS derivative function with a confinement-dependent 3D implementation method previously formulated and validated for temperatures up to 250 °C by the authors [17].

The obtained LITS constitutive relationship is here calibrated and validated against transient tests performed under uni- and bi-axial compression for temperatures up to 500 °C. The validated method is next used to assess the structural behaviour of a PCPV subjected to 2 and 14-day long accidental fault conditions.

The following conclusions can be drawn:

- If a LITS derivative function that accurately assesses LITS development for uniaxial conditions is extended to 3D with the traditional confinement-independent approach, erroneous results are obtained. In particular, the LITS that develops in both the loaded and unloaded directions in the case of multiaxial compressive stress states is significantly underestimated. This was previously demonstrated by the authors with a bilinear LITS derivative curve for temperatures up to 250 °C [17] and is here illustrated with a polynomial LITS derivative curve for temperatures up to 500 °C.
- If the same uniaxial LITS derivative function is extended to 3D via the confinement-dependent implementation approach adopted here, a better prediction of the experimentally observed LITS curves is obtained for temperatures up to 500 °C. Consequently, a better assessment of the total thermal strain, seen as the sum of FTS and LITS, is provided.
- In the case of numerical modelling of PCPVs subjected to severe accidental fault conditions, the inclusion of a LITS model in the constitutive relationship is key to capturing the actual stress redistribution taking place in concrete and prestressing tendons. If LITS is not included, significant losses in the tendons pretension, corresponding to losses in concrete precompression, are missed. Moreover, these losses are significantly underestimated if LITS is implemented in 3D via the traditional confinement-independent method.
- The mechanical behaviour of PCPV subjected to severe accidental conditions strongly depends on the duration of the fault.
- The presented LITS constitutive relationship can readily be included in existing concrete material models that include damage, plasticity and creep.

Acknowledgements

This work was supported by EPSRC and EDF Energy.

References

[1] Illston JM, Sanders PD. Effect of temperature change upon the creep of mortar under torsional loading. Mag Concr Res 1973;25:136–44.
[2] Illston JM, Sanders PD. Chatacteristics and prediction of creep of a saturated mortar under variable temperature. Mag Concr Res 1974;26:169–79.
[3] Parrott LJ. Study of transitional thermal creep in hardened cement paste. Mag Concr Res 1979;31:99–103.

[4] Fahmi HM, Polivka M, Bresler B. Effects of sustained and cyclic elevated temperature on creep of concrete. Cem Concr Res 1972;2:591–606. doi:10.1016/0008-8846(72)90113-5.
[5] Colina H, Sercombe J. Transient thermal creep of concrete in service conditions at temperatures up to 300 °C. Mag Concr Res 2004;56:559–74.
[6] Hassen S, Colina H. Transient thermal creep of concrete in accidental conditions at temperatures up to 400 °C. Mag Concr Res 2006;58:201–8. doi:10.1680/macr.2006.58.4.201.
[7] Mindeguia J-C, Hager I, Pimienta P, Carré H, La Borderie C. Parametrical study of transient thermal strain of ordinary and high performance concrete. Cem Concr Res 2013;48:40–52.
[8] Petkovski M, Crouch RS. Strains under transient hygro-thermal states in concrete loaded in multiaxial compression and heated to 250 °C. Cem Concr Res 2008;38:586–96.
[9] Law A, Gillie M. Load induced thermal strains: implications for structural behaviour. In: Proceedings of the 5th international conference on structures in fire; 2008.
[10] de Borst R, Peeters PPJM. Analysis of concrete structures under thermal loading. Comput Methods Appl Mech Eng 1989;77:293–310. doi:10.1016/0045-7825(89)90079-0.
[11] Gawin D, Pesavento F, Schrefler BA. Modelling of deformations of high strength concrete at elevated temperatures. Mater Struct Constr 2004;37:218–36.
[12] Khennane A, Baker G. Thermoplasticity model for concrete under transient temperature and biaxial stress. Proc R Soc Lond A Math Phys Eng Sci 1992;439:59–80.
[13] Thelandersson S. Modeling of combined thermal and mechanical action in concrete. J Eng Mech 1987;113:893–906.
[14] Pearce CJ, Nielsen CV, Bićanić N. Gradient enhanced thermo-mechanical damage model for concrete at high temperatures including transient thermal creep. Int J Numer Anal Methods Geomech 2004;28:715–35. doi:10.1002/nag.376.
[15] Gernay T, Millard A, Franssen J-M. A multiaxial constitutive model for concrete in the fire situation: theoretical formulation. Int J Solids Struct 2013;50:3659–73. doi:10.1016/j.ijsolstr.2013.07.013.
[16] Kordina K, Ehm C, Schneider U. Effects of biaxial loading on the high temperature behaviour of concrete. Fire Saf Sci 1986;1:281–90. doi:10.3801/IAFSS.FSS.1-281.
[17] Torelli G, Gillie M, Mandal P, Tran V-X. A multiaxial load-induced thermal strain constitutive model for concrete. Int J Solids Struct 2016. doi:10.1016/j.ijsolstr.2016.11.017.
[18] Khoury GA, Grainger BN, Sullivan PJE. Strain of concrete during first heating to 600 °C under load. Mag Concr Res 1985;37:195–215.
[19] Torelli G, Mandal P, Gillie M, Tran V-X. Concrete strains under transient thermal conditions: a state-of-the-art review. Eng Struct 2016;127:172–88. doi:10.1016/j.engstruct.2016.08.021.
[20] Li L, Purkiss J. Stress–strain constitutive equations of concrete material at elevated temperatures. Fire Saf J 2005;40:669–86. doi:10.1016/j.firesaf.2005.06.003.
[21] Diederichs U. Modelle zur Beschreibung der Betonverformung bei instantion{ä}ren Temperaturen. Abschlu{ß}kolloq–Bauw Unter Brand 1987:25–34.
[22] Terro MJ. Numerical modeling of the behavior of concrete structures in fire. ACI Struct J 1998;95:183–93.
[23] Anderberg Y, Thelandersson S. Stress and deformation characteristics of concrete at high temperature: 2. Experimental investigation and material behaviour model. Bull. Div. Struct. Mech. Concr. Constr. Bull. 54, Lund: 1976, p. 86.
[24] De Soza T Code_Aster: guide de lecture de la documentation de référence http://www.code-aster.org.
[25] Helfer T, Michel B, Proix J-M, Salvo M, Sercombe J, Casella M. Introducing the open-source mfront code generator: Application to mechanical behaviours and material knowledge management within the PLEIADES fuel element modelling platform. Comput Math Appl 2015;70:994–1023. doi:10.1016/j.camwa.2015.06.027.
[26] Zienkiewicz OC. The finite element method. London: McGraw-hill; 1977.
[27] EDF. Algorithme Non Linéaire Quasi-Statique STAT_NON_LINE Référence du Code Aster R5.03.01 révision : 10290. http://www.code-aster.org.
[28] Hilsdorf H. Die Bestimmung der zweiachsigen Festigkeit des Betons. Ernst; 1965.
[29] Thelandersson S. Mechanical behaviour of concrete under torsional loading at transient, high-temperature conditions. Bull. Div. Struct. Mech. Concr. Constr. Concr. Constr. Bullettin 46, Lund: 1974, p. 83.
[30] Schneider U, Kordina K. On the bahaviour of normal concrete under steady state and transient temperature conditions. H - Struct. Anal. Prestress. Concr. React. Press. Vessel. H1 - Concr. Prop. Relev. to PCRV. SMiRT 3, London, UK: IASMiRT; 1975.
[31] EN, BS. 1-2: 2004 Eurocode 2: Design of concrete structures-Part 1-2: General rules-Structural fire design. Eur Stand 2004.
[32] Granger L. Comportement différé du béton dans les enceintes de centrales nucléaires. Analyse et modélisation. PhD Thesis. Ecole Nationale des Ponts et Chaussées, 1996.